arXiv:1412.7230v1 [astro-ph.SR] 23 Dec 2014

On the oxygen abundances of M 67 stars from the turn-off point through the red-giant branch *

Yoichi Takeda[1,2] and Satoshi Honda[3]

[1] *National Astronomical Observatory, 2-21-1 Osawa, Mitaka, Tokyo 181-8588*

takeda.yoichi@nao.ac.jp

[2] *The Graduate University for Advanced Studies, 2-21-1 Osawa, Mitaka, Tokyo 181-8588*

[3] *Nishi-Harima Astronomical Observatory, Center for Astronomy, University of Hyogo, 407-2 Nishigaichi, Sayo-cho, Sayo, Hyogo 679-5313*

(Received 2014 October 8; accepted 2014 December 18)

Abstract

With an aim to examine whether the surface oxygen composition suffers any appreciable change due to evolution-induced mixing of nuclear-processed material in the envelope of red giants, abundance determinations for O/Fe/Ni based on the synthetic spectrum-fitting method were performed by using the moderate-dispersion spectra in the 7770–7792Å region (comprising O I 7771–5, Fe I 7780, and Ni I 7788 lines) for 16 stars of the old open cluster M 67 in various evolutionary stages from the turn-off point through the red giant branch. We could not find any meaningful difference in the oxygen abundances between the non-giant group ($T_{\rm eff} > 5000$ K) and the red-giant group ($T_{\rm eff} < 5000$ K), which are almost consistent with each other on the average (despite that both have rather large dispersions of a few tenths dex caused by insufficient data quality), though only one giant star (S 1054) appears to show an exceptionally low O abundance and thus needs a more detailed study. This result may suggest that oxygen content in the stellar envelope is hardly affected (or changes are insignificant) by the mixing of H-burning products in the red-giant phase, as far as M 67 stars of low mass ($\sim 1.3 M_{\odot}$) are concerned, which is consistent with the prediction from the conventional stellar evolution theory of first dredge-up.

Key words: open clusters and associations: individual: M 67 — stars: abundances — stars: atmospheres — stars: evolution — stars: late-type

* Based on data collected by using the NAYUTA Telescope of the Nishi-Harima Astronomical Observatory.

1. Introduction

As a star is evolved off the main sequence after exhaustion of hydrogen fuels in the core, it increases its radius while the surface temperature drops down, and the deep convection zone is developed. As a result, some portion of the H-burning (CNO cycle) product in the interior may be salvaged and mixed to alter the surface abundances of red giants. According to the canonical stellar evolution calculation, it is essentially the CN-cycled (C→N reaction) material that is dredged up, while the product of ON-cycle (O→N reaction; occurring in deeper region of higher T) is unlikely to cause any significant abundance change because mixing is not expected to substantially penetrate into such a deep layer; thus the predicted surface abundances are characterized by a deficit in C as well as an enhancement in N (with its peculiarity degree increasing with mass/luminosity), while O is practically unaffected (see, e.g., Fig. 24 in Mishenina et al. 2006).

While such expected tendency has been almost confirmed observationally for C and N, the behavior of O is still controversial and unsettled:
— Mishenina et al. (2006) reported that the oxygen abundances (determined based on the [O I] forbidden line at 6300 Å) in red-clump giants of $\sim$ 1–3 $M_\odot$ are almost normal ($\langle$[O/Fe]$\rangle \simeq 0$), in agreement with the theoretical prediction.
— Further, Tautvaišienė et al.'s (2010) similar study on red-clump giants resulted in essentially the same conclusion as Mishenina et al.'s.
— However, Takeda, Sato, and Murata (2008) reported in their extensive spectroscopic analysis of 322 late-G and early-K giants (4500 K $\lesssim T_{\rm eff} \lesssim$ 5500 K, 1.5 $\lesssim \log g \lesssim$ 3.5, 1 $\lesssim M/M_\odot \lesssim$ 5) that [O/Fe] (determined from [O I] 5577 line) shows a subsolar tendency with the extent of peculiarity increasing with M (cf. figure 12 therein), which implies that a mass-dependent dredge-up of (not only CN-cycle but also) ON-cycle products may take place in the envelope of red giants. So, if this is real, it would require a revision of the standard theory for the dredge-up in the envelope of red giants.

The best approach to check whether or not stellar surface abundances suffer changes during the evolutionary paths from the main sequence to the red giant phase is to investigate a number of stars (of various types) belonging to an open cluster. That is, since all such member stars are considered to have the same age as well as the same initial composition, detection of any systematic abundance differences along the evolutionary sequence would make a direct evidence for the existence of evolution-induced build-up of chemical peculiarity. Above all, the well known old open cluster M 67 (NGC 2682) is especially suitable for this purpose, since (unlike many other comparatively young clusters) it has a particular merit of including a wealth of stars (not only on the main sequence but also) on the continuous evolutionary sequence from the turn-off point through the red-giant branch.

This well known old Galactic cluster has been repeatedly studied and several reports on

the oxygen abundances of M 67 member stars are already available; e.g., Brown (1985) for 3 giants; Shetrone and Sandquist (2000) for 10 blue-straggler and turn-off stars; Tautvaišienė et al. (2000) for 10 giants; Yong, Carney and Teixera de Almeida (2005) for 3 giants; Randich et al. (2006) for 10 dwarfs/subgiants of late F- and early G-type; Pace, Pasquini, and François (2008) for 5 solar-type stars; Pancino et al. (2010) for 3 giants.[1] However, any trial of systematic oxygen abundance studies in a consistent manner for a wide range of M 67 stars from near-main sequence (F type) through red giants (K type) has never been made so far to our knowledge.

Motivated by this situation, we decided to conduct a spectroscopic study on M 67 stars in various stages from less evolved (near to turn-off points) through fully evolved (red giants), in order to determine their oxygen abundances based on O I 7771–5 triplet lines (by making use of the fact that these O I lines are visible in a wide range of stars from spectral type A through K) and to see if any systematic oxygen abundance peculiarity (e.g., a comparative deficit of O in red giants) is observed. This was our primary purpose.

Somewhat disappointingly, we realized in the course of the analysis that the spectral data we obtained for the relevant M 67 stars of $V \lesssim 13$ mag with the 2-m NAYUTA telescope (used for this study) were of insufficient quality (i.e., S/N ratios were from only several tens to ~ 100) to carry out reliable abundance determinations. Yet, we positively considered that this is a good opportunity for us to learn how much abundance information is gained by carefully studying rather noisy spectra of medium resolution, since such circumstances may be encountered in astronomical spectroscopy of faint objects. Accordingly, we paid special attention to quantitatively estimating errors involved in the resulting abundances. This challenge makes another aim of this investigation.

The remainder of this article is organized as follows. After describing our observations in section 2, we explain the assignments of stellar parameters in section 3. The procedure of our abundance determination based on the spectrum-fitting method is illustrated in section 4, followed by section 5 where abundance errors are evaluated in various respects. The resulting abundances are discussed in section 6, and the conclusion is summarized in section 7.

2. Observational data

The list of our 16 targets of M 67 cluster is presented in table 1, which were selected to cover the evolutionary status from the turn-off point through the red-giant branch (cf. figure 2a). Spectroscopic observations of these stars were carried out in 2014 January and February using the Medium And Low-dispersion Longslit Spectrograph (MALLS; cf. Ozaki & Tokimasa 2005) installed on the Nasmyth platform of the 2-m NAYUTA telescope at Nishi-Harima Astronomical Observatory (NHAO). Equipped with a 2K×2 K CCD detector (13.5

[1] We do not pay attention here to the pioneering studies done in 1970's based on photographic plates because of their less reliability; see, e.g., Sect. 1 of Tautvaišienė et al. (2000).

μm pixel), MALLS can record a spectrum covering $\sim$ 400 Å (7600–8000 Å) in the medium-resolution mode with the resolving power of $R \sim 12000$. Since we had to limit the maximum exposure time of one frame up to 20 minutes (because of enhanced dark level), a number of spectral frames were co-added in order to reduce the spectrum noise as much as possible. The reduction of the spectra (bias subtraction, flat-fielding, spectrum extraction, wavelength calibration, co-adding of frames to improve S/N, continuum normalization) was performed by using the "noao.onedspec" package of the software IRAF[2] in a standard manner.

The S/N ratios of the resulting spectra were estimated in two ways. First, assuming the photon-noise-limited case, we derived S/N(predicted) $\simeq \sqrt{n_{\rm ph}}$ ($n_{\rm ph}$ is the photon counts). Second, we directly measured the standard deviation (σ_k) and the average ($\langle c_k \rangle$) of the spectrum at each of the selected eight line-free windows (k) of several Å width, which gives the local S/N for region k as $({\rm S/N})_k \equiv \langle c \rangle_k / \sigma_k$. We then averaged each $({\rm S/N})_k$ to obtain S/N(measured) while weighting according to $w_k (\propto \sigma_k^{-2})$. The correlation between S/N(predicted) and S/N(measured) is shown in figure 1, where we can see that both are reasonably correlated with each other (though quantitative agreement is not necessarily good). From a modest standpoint, we adopted (the rounded value of) the smaller one of these two S/N ratios for each star. Unfortunately, the finally achieved S/N ratios were not satisfactory. While moderate values of $\sim$ 100 were realized for brighter giant stars, we could gain only several tens for the case of fainter turn-off stars of $V \gtrsim 12.5$. Accordingly, since the spectrum quality is not sufficient for reliable abundance determination, we must carefully check how much errors are involved in the resulting abundances, as will be done in section 5. The observational data (observed date, exposure time, S/N) of these M 67 stars are summarized in table 1.

Besides, we also observed Pollux (K0 III), Procyon (F5 IV–V), and Ganymede (substitute for the Sun) as the reference stars, for which the spectra turned out to be of sufficiently high quality (S/N of more than several hundreds). Our spectra in the 7680–7820 Å region are displayed in figure 3 for each of the 19 program stars.

3. Stellar parameters

Regarding the common properties of M 67 member stars, we adopted [Fe/H] = +0.02 (metallicity), $E(B-V) = +0.04$ (color excess), and $(m-M)_0 = 9.60$ (true distant modulus), following Sandquist (2004). The effective temperature ($T_{\rm eff}$) was evaluated from dereddened $(B-V)_0$ [$\equiv (B-V) - E(B-V)$] by invoking Alonso, Arribas, and Martínez-Roger's (1996) equation (1) as well as Alonso, Arribas, and Martínez-Roger's (1999) table 2 for 7 non-giants ($B-V < 0.9$) and 9 giants ($B-V > 0.9$), respectively. The bolometric luminosity (L) was derived from the absolute magnitude M_V [$\equiv V - (m-M)_0 - 3.1E(B-V)$] and the bolometric

[2] IRAF is distributed by the National Optical Astronomy Observatories, which is operated by the Association of Universities for Research in Astronomy, Inc. under cooperative agreement with the National Science Foundation.

correction (B.C.) calibrated by Alonso, Arribas, and Martínez-Roger (1995) as well as Alonso et al. (1999) for non-giants and giants, respectively. As such, our M 67 targets are plotted on the $\log L$ vs. $\log T_{\rm eff}$ diagram shown in figure 2b, where Demarque et al.'s (2004) Yale–Yonsei theoretical solar-metallicity evolutionary tracks (Y2_tracks_a0o2newOS.gz[3]) as well as the 4 Gyr isochrone (YYiso_v2.tar.gz[4]) are also drawn.

The surface gravity ($\log g$) of each star was then calculated as

$$\log(g/g_{\odot}) = \log(M/M_{\odot}) - \log(L/L_{\odot}) + 4\log(T_{\rm eff}/T_{\rm eff\odot}) \quad (1)$$

where those with subscript "$\odot$" are the solar values and we adopted $M = 1.3 M_{\odot}$ (cf. figure 1b).

Regarding the microturbulence ($v_{\rm t}$), Takeda et al.'s (2013) empirical formula (cf. equation (1) and equation (2) therein) was adopted for non-giants ($T_{\rm eff} > 5000$ K). As to giants ($T_{\rm eff} < 5000$ K), we assumed a $\log g$-dependent relation

$$v_{\rm t} = 0.01 + 1.30 \log g - 0.31 (\log g)^2 \quad (2)$$

(where $v_{\rm t}$ is in km s^{-1} and g is in cm s^{-2}), which we found to well represent (within $\sim \pm$ 0.1–0.2 km s^{-1}) the $v_{\rm t}$ data derived by Takeda et al. (2008; cf. figure 1c therein) for giants in the parameter range of 4600 K $< T_{\rm eff} <$ 4900 K and $2.3 < \log g < 3.3$.

Concerning the reference stars, we assigned ($T_{\rm eff}$, $\log g$, [Fe/H], and $v_{\rm t}$) as follows: (4904 K, 2.84, +0.06, and 1.3 km s^{-1}) for Pollux (Takeda et al. 2008), (6612 K, 4.00, −0.02, and 2.0 km s^{-1}) for Procyon (Takeda et al. 2005), and (5780 K, 4.44, 0.00, and 1.0 km s^{-1}) for the Sun. These finally adopted atmospheric parameters for each star are summarized in table 2. Besides, how the $\log g$ and $v_{\rm t}$ of our M 67 targets depend characteristically upon $T_{\rm eff}$ is displayed in figure 4.

Such assigned parameters are compared in table 3 with those adopted in previous investigations on oxygen abundances in M 67 (cf. section 1), where five M 67 stars common to our sample were analyzed in four studies. We can see from this table that both are reasonably consistent with each other in terms of $T_{\rm eff}$ and $\log g$, since the differences are $\lesssim 50$ K and $\lesssim 0.1$ dex in most cases, respectively (except that Pancino et al.'s spectroscopic $\log g$ for S 1010 is by ~ 0.4 dex higher while their photometric $\log g$ is in agreement with ours). Regarding $v_{\rm t}$ for giants, Tautvaišienė et al. (2000) used systematically higher values (1.7–1.8 km s^{-1}) than that (1.3 km s^{-1}) adopted by us, while Yong et al.'s (2005) $v_{\rm t}$ (1.34 km s^{-1} for S 1010) is consistent with ours.

[3] ⟨http://www.astro.yale.edu/demarque/yystar.html⟩.

[4] ⟨http://csaweb.yonsei.ac.kr/~kim/yyiso.html⟩.

4. Abundance determinations

4.1. Model atmospheres and spectral line data

The model atmosphere for each star to be used for abundance derivations was constructed by three-dimensionally interpolating Kurucz's (1993) ATLAS9 model grid in terms of $T_{\rm eff}$, $\log g$, and [Fe/H]. Regarding the atomic parameters of spectral lines, we basically invoked the extensive compilation by Kurucz and Bell (1995), while applying appropriate adjustments to $\log gf$ values when necessary (see footnote 5 and note in table 4). By using these atmospheric models, we simulated the theoretical spectra in the 7680–7820 Å region while assuming the metallicity-scaled solar abundances for all elements (and convolved them with the Gaussian broadening function corresponding to $R \sim 12000$), which are overplotted in figure 3.[5]

4.2. Spectrum-fitting analysis

A three-step procedure based on the spectrum-fitting technique was adopted for oxygen abundance determination, the main theme of this study. This is because that directly measuring the equivalent widths of O I 7771–5 lines is not easy because of their weakness (especially for giant stars) as well as appreciable noises due to insufficient quality of our spectra:
— (i) First, we fitted the theoretical synthetic spectrum with the observed spectrum by finding the most optimal (LTE) abundance solutions of $A^{\rm L}$(O),$A^{\rm L}$(Fe), and $A^{\rm L}$(Ni) (along with the macro-broadening width $v_{\rm M}$ and the radial velocity), while applying the automatic fitting algorithm (Takeda 1995) to the 7770–7792 Å region (comprising O I 7771–5, Fe I 7780, and Ni I 7788 lines). The adopted atomic data of the relevant O I, Fe I, and Ni I lines are summarized in table 4, for which we invoked Kurucz and Bell's (1995) compilation. However, only the $\log gf$ value (-0.066) for the Fe I line at 7780.552 Å was exceptionally taken from Kurucz and Peytremann's (1975) old database as done by Takeda and Sadakane (1997), since the value (-2.361) given in Kurucz and Bell (1995) is too small and apparently inappropriate (it would lead to an unrealistically large solar Fe abundance). Since we could not arrive at any converged solution for S 1288 and S 1056 because lines are overwhelmed by noises, we abandoned A(O)

[5] In this computation, we basically adopted Kurucz and Bell's (1995) compilation for the atomic data. We noticed, however, that their original gf values were not necessarily appropriate for quite a few lines in this wavelength region, to which adequate adjustments must be applied in order to accomplish a satisfactory match between theory and observation. Accordingly, we estimated the necessary corrections ($\Delta \log gf$) for the following 17 lines by comparing the observed spectrum of Ganymede and the theoretical solar flux spectrum simulated with the standard solar abundances: Ni I 7715.583 (by +1.0 dex), S I 7725.046 (by −0.7 dex), Fe I 7742.685 (by +0.3 dex), Si I 7745.101 (by −0.5 dex), Mg I 7746.345 (by −1.3 dex), Si I 7750.010 (neglected), Fe I 7770.279 (by −0.7 dex), Ca I 7771.239 (neglected), Fe I 7771.427 (by −0.7 dex), Fe I 7772.597 (by −0.1 dex), Ti I 7773.904 (neglected), Fe I 7774.001 (by +1.5 dex), Ca I 7775.496 (neglected), Ca I 7775.763 (neglected), Fe I 7780.552 (by +2.3 dex; see also table 4), Si I 7799.180 (neglected), and Si I 7799.996 (by +1.5 dex). Besides, 6 additional CN lines in the 7770–7777 Å region used by Takeda, Sadakane, and Kawanomoto (1998) were also included with Eriksson and Toft's (1979) gf values.

determinations for these two stars. The eventually accomplished fit for each spectrum is shown in figure 5, and the results of $A^{\rm L}$(O),$A^{\rm L}$(Fe), and $A^{\rm L}$(Ni) are given in table 2.
— (ii) Second, the equivalent width (EW_{7774}) of the O I line at 7774.17 Å (the middle line of the triplet) was *inversely* computed from such established solution of $A^{\rm L}$(O) by using the same model atmosphere.[6] Similarly, EW_{7780} and EW_{7788} for Fe I 7780.55 and Ni I 7788.94 lines were derived from $A^{\rm L}$(Fe) and $A^{\rm L}$(Ni).
— (iii) Finally, regarding oxygen, the non-LTE correction for O I 7774.17 ($\Delta^{\rm N}_{7774}$) was evaluated from EW_{7774} by following the procedure described in Takeda (2003), which was applied to $A^{\rm L}$(O) (derived in step (i)) to obtain $A^{\rm N}$(O) (non-LTE oxygen abundance) as $A^{\rm N}({\rm O}) = A^{\rm L}({\rm O}) + \Delta^{\rm N}_{7774}$.[7] Such obtained results of $\Delta^{\rm N}_{7774}$ and $A^{\rm N}$(O) are also presented in table 2.

5. Error analysis

In the present case where spectra of insufficient quality are used, the primary source of errors accompanied with our abundance results is due to noises. We estimated this kind of abundance error by two independent ways: (1) Based on expected uncertainties in the equivalent widths, and (2) directly analyzing a number of mock spectra (with artificially added noises) in the same spectrum-fitting method. Besides, we also have to evaluate errors due to ambiguities in the adopted atmospheric parameters ($T_{\rm eff}$, $\log g$, and $v_{\rm t}$).

5.1. Noise-related error #1: based on equivalent widths

Regarding the error in EW, we invoked the formula derived by Cayrel (1988)

$$\delta EW \simeq 1.6 (w \delta x)^{1/2} \epsilon, \tag{3}$$

where δx is the pixel size (0.21 Å), w is the full-width at half maximum (corresponding to $\simeq 25$ km s^{-1} or $R \simeq 12000$), and $\epsilon \equiv ({\rm S/N})^{-1}$. We thus determined the abundances for each of the perturbed $EW_+ (\equiv EW + \delta EW)$ and $EW_- (\equiv EW - \delta EW)$, respectively, from which the

[6] Actually, this computation was done also for the other two lines of the triplet at 7771.94 and 7775.39 Å. These EW_{7771} and EW_{7775} are well correlated with EW_{7774} through the following relations: $EW_{7771} = 0.1 + 1.18 EW_{7774} + 5.61 \times 10^{-4} EW^2_{7774}$ and $EW_{7775} = 0.3 + 0.76 EW_{7774} + 7.70 \times 10^{-4} EW^2_{7774}$, where EW's are expressed in mÅ. Naturally, he inequality relation $EW_{7771} > EW_{7774} > EW_{7775}$ always holds between these three EWs, reflecting the difference of $\log gf$.

[7] We may regard the oxygen abundance derived from the O I 7774.17 line (the middle component) practically equivalent to that corresponding to the O I 7771–5 triplet as a whole for the following reason. The non-LTE abundance for the triplet (the mean of $A^{\rm N}_{7771}$, $A^{\rm N}_{7774}$, and $A^{\rm N}_{7775}$) is expressed as $\langle A^{\rm N} \rangle \equiv A^{\rm L} + (\Delta^{\rm N}_{7771} + \Delta^{\rm N}_{7774} + \Delta^{\rm N}_{7775})/3$, where the inequality relation $|\Delta^{\rm N}_{7771}| > |\Delta^{\rm N}_{7774}| > |\Delta^{\rm N}_{7775}|$ generally holds for the extents of (negative) non-LTE correction according to Takeda (2003) because of the difference in the component strengths ($EW_{7771} > EW_{7774} > EW_{7775}$; cf. footnote 6). We actually found the following equations regarding the $\Delta^{\rm N}$ values of each lines derived for our the program stars: $\Delta^{\rm N}_{7771} \simeq 1.10 \Delta^{\rm N}_{7774}$ and $\Delta^{\rm N}_{7775} \simeq 0.85 \Delta^{\rm N}_{7774}$. Given this situation, the difference between $\Delta^{\rm N}_{7774}$ and $(\Delta^{\rm N}_{7774} + \Delta^{\rm N}_{7774} + \Delta^{\rm N}_{7775})/3$ turned out to be very small and negligible (< 0.01 dex for all stars), by which we can state that $A^{\rm N}_{7774}$ is essentially equivalent to $\langle A^{\rm N} \rangle$.

differences from the standard A were derived as $\delta A_+(>0)$ and $\delta A_-(<0)$.

5.2. Noise-related error #2: based on artificial spectra

We first calculated the reference spectrum corresponding to the standard solutions of A_0(O),A_0(Fe), A_0(Ni), and $v_{\rm M0}$ for each star (obtained in subsection 4.2). Then, randomly-generated noises of normal distribution (corresponding to the S/N ratio) were added to this standard spectrum, and this process was repeated 100 times. In this way, 100 artificial spectra were generated, as shown in figure 6. Next, we tried abundance determinations in exactly the same manner as described in subsection 4.2, and obtained A_i(O), A_i(Fe), and A_i(Ni) for each spectrum i (i = 1, 2, $\cdots$, 100), The distributions of the resulting A_i(O) are illustrated in figure 7. Then, from this ensemble of A_i, the average $\langle A \rangle$ and the standard deviation (σ_A) were computed. We can regard this σ_A (representing the dispersion of A_i) as an estimate of abundance errors caused by noises.

5.3. Effect of atmospheric parameters

The uncertainties in A due to errors of atmospheric parameters were evaluated by repeating the analysis on EW while perturbing the standard values of atmospheric parameters interchangeably by $\pm$2% in $T_{\rm eff}$ (typical differences between various determinations; cf. Takeda et al. 2005, 2008), $\pm$0.1 dex in $\log g$ (typical differences between spectroscopic $\log g$ and directly determined $\log g$ as adopted in this study; cf. Takeda et al. 2005, 2008), and $\pm$20% in $v_{\rm t}$ (typical scatter around the analytical formula used by us). We call these six kinds of abundance variations as δ_{T+}, δ_{T-}, δ_{g+}, δ_{g-}, δ_{v+}, and δ_{v-}, respectively.

5.4. Trend of each error source

These abundance errors derived in the last three subsections [(δA_-, δA_+), ($-\sigma_A$, $+\sigma_A$), (δ_{T+}, δ_{T-}), (δ_{g+}, δ_{g-}), (δ_{v+}, and δ_{v-})] along with equivalent widths (EW) are graphically shown as functions of $T_{\rm eff}$ in figures 8 (O), 9 (Fe), and 10 (Ni). In figure 8, the non-LTE corrections ($\Delta^{\rm N}_{7774}$) are also plotted for comparison.

We can see from these figures the following trends:

— The noise-related errors (δA or σ_A) are quantitatively more significant than the parameter-related ones in the present case.

— Reflecting the fact that they are of the same origin, $|\delta A|$ and σ_A are almost of the same extent. though the former tends to be somewhat larger than the latter.

— Regarding the parameter-related errors, δ_T's are more or less appreciable (particularly for O in red giants), δ_g's are negligibly small, and δ_v's are important only for Fe and Ni (especially in red giants).

— The extents of (negative) non-LTE correction for O I 7774 are considerably EW-dependent, and range from $\sim$ 0.1 dex (red giants) and $\sim$ 0.4–0.5 dex (turn-off stars).

For evaluating the total error budget, we adopt σ_A (which is more preferable than δA

from the viewpoint of authenticity in the derivation procedure) for S/N-related error and $\delta_{Tgv}[\equiv (\delta_T^2+\delta_g^2+\delta_v^2)^{1/2}]$ for parameter-related error (where δ_T is the average of $|\delta_{T+}|$ and $|\delta_{T-}|$; and the same applies also for δ_g and δ_v). That is, we regard $\pm\sqrt{\sigma_A^2+\delta_{Tgv}^2}$ as the error bars attached to the abundance results obtained in section 4 (cf. table 2). Our final abundances of O, Fe, and Ni (with such estimated error bars) are plotted against $T_{\rm eff}$ in figure 11, where the results for Pollux, Procyon and Sun are shown for comparison.

6. Discussion

6.1. Abundances of Fe and Ni

We first review the abundances of Fe and Ni (iron-group elements representative of the metallicity) for M 67 stars shown in figure 11b and figure 11c. Dividing all 16 stars into giant group ($T_{\rm eff} < 5000$ K; 9 stars) and non-giant group ($T_{\rm eff} > 5000$ K; 7 stars), we obtain $\langle A({\rm Fe})\rangle$(giant) = 7.57($\pm$0.39), $\langle A({\rm Fe})\rangle$(non-giant) = 7.61($\pm$0.58), and $\langle A({\rm Fe})\rangle$(all) = 7.59($\pm$0.44) as the averaged abundances of Fe for each group (values in parentheses after $\pm$ are the standard deviations). Meanwhile, the results for Ni are $\langle A({\rm Ni})\rangle$(giant) = 6.40($\pm$0.43), $\langle A({\rm Ni})\rangle$(non-giant) = 6.44($\pm$0.55), and $\langle A({\rm Ni})\rangle$(all) = 6.42($\pm$0.47). These results suggest that (i) A(Fe) and A(Ni) do not show any systematic dependence upon $T_{\rm eff}$, and (ii) they are more or less consistent with those of the standard stars (Pollux, Procyon, and Sun) within the dispersion, which can also be recognized by eye-inspection of figure 11b and figure 11c, even though appreciable scatters amounting to $\pm$ 0.4–0.5 dex are seen. Accordingly, we may state that the derived abundances of Fe and Ni for M 67 stars do not show any systematic trend, which does not contradict the uniformity in the metallicity within this cluster. This, in turn, may imply that the atmospheric parameters which we assigned to each star are almost reasonable.

6.2. O abundances in M 67: almost uniform but one exception

Our non-LTE oxygen abundances, which are plotted against $T_{\rm eff}$ in figure 11a, appear to show nearly the same trend seen for Fe and Ni (figure 11b and figure 11c). That is, A(O) values do not show any systematic dependence upon $T_{\rm eff}$ and are almost consistent with those of standard stars, which means that almost the same argument as given in subsection 6.1 may hold also for this case of oxygen. We notice, however, that only one star (S 1054) exhibits conspicuously low A(O) compared to other M 67 stars by $\sim$1 dex. Excluding this S 1054, we obtain $\langle A({\rm O})\rangle$(giant but S1054) = 8.55($\pm$0.19), $\langle A({\rm O})\rangle$(non-giant) = 8.63($\pm$0.46), and $\langle A({\rm O})\rangle$(all but S1054) = 8.59($\pm$0.33).[8] Such derived mean abundance ($\sim$ 8.6) is reasonably consistent with those of Pollux (8.43), Procyon (8.84), and Sun (8.60) within $\lesssim$ 0.2 dex. Accordingly, we may

[8] That the abundance dispersion in non-giant group (0.46 dex) is appreciably larger than that in giant group (0.19 dex) is apparently due to the poor spectrum quality for the former group (note that we had to use data with S/N ratios as low as $\sim$ 20–30; cf. table 1).

conclude that atmospheric oxygen abundances of M 67 stars studied by us are almost uniform (with one exception) at the near-solar composition[9] irrespective of the evolutionary phase from unevolved turn-off stars through well-evolved red giants. This may be regarded as a significant consequence, given that the O I line strengths in our M 67 samples widely differ from each other (by a factor amounting up to ~ 10; cf. figure 8a).

6.3. On the nature of S 1054

The outlier behavior of A(O) for S 1054 is curious. Is this an unusual star compared to other M 67 members? While Sandquist (2004) classified this star as "RGB binary?", its position on the HR diagram is not peculiar as compared to other red giants, which makes it less likely that this star actually be an unresolved binary. This argument is substantiated by the fact that its heliocentric radial velocities ($V_{\rm r}^{\rm hel}$) at 20 different dates over the time span of ~ 5400 days reported by Mathieu et al. (1986) are quite stable; i.e., $\langle V_{\rm r}^{\rm hel}\rangle = 33.5$ km s^{-1} with a standard deviation of only 0.4 km s^{-1}. Besides, it is almost no doubt that S 1054 belongs to M 67 membership, as this $\langle V_{\rm r}^{\rm hel}\rangle$ is reasonably consistent with those of other members. Accordingly, we can not help considering that S 1054 is an ordinary red giant star of M 67. Then, how should we interpret its markedly low A(O) (7.37) for this star compared with the others (~ 8.6 on the average)? Here, we should recall that the error accompanied with A(O) of S 1054 derived in subsection 5.4 is appreciably large to be $\pm 0.50 (\equiv \pm\sqrt{\sigma_A^2 + \delta_{Tgv}^2})$ despite that spectrum S/N ratio of ~ 100 is sufficiently high, because the O I 7771–5 lines are considerably weak. Therefore, the disagreement of ~ 1.2 dex corresponds to $\sim 2.4\sigma$, which means that a small probability of a few per cent[10] still remains that this large discrepancy is due to a random fluctuation. In any case, this star is worth special attention, for which further study based on high-quality spectrum is eagerly awaited. If this marked O-deficiency were real, this would make a very interesting object.

6.4. Does evolution-induced mixing have impact on surface oxygen in red giants?

Let us discuss the implication of this result from the viewpoint of our original motivation (i.e., to check the theoretical prediction in comparison with the observational fact). According the recent calculation of Lagarde et al. (2012), the logarithmic oxygen abundance ratio ([O/H]) of a solar-metallicity 1.25 $M_\odot$ star at the red-giant phase is only -0.001 (case 1: standard recipe) and -0.0013 (case 2: including thermohaline convection and rotation-induced mixing); i.e., essentially unaffected by the mixing of H-burning products for both of the cases considered by them. In this sense, our observational consequence (no meaningful difference between the O

[9] Regarding two stars (S 1288 and S 1056), for which A(O) could not be determined, their spectrum feature at the position of O I lines (severely affected by noises) does not contradict the normal oxygen composition, as shown in figure 5, where we assumed [O/Fe] = 0 as fixed for these two stars.

[10] In the case of normal (Gaussian) error distribution, the probability that a deviation of $\geq 2\sigma$ occurs is 0.046 ($= 1 - \mathrm{erf}(2)$).

abundances of evolved red giants and unevolved or less evolved stars) is fully consistent with such theoretical expectations, as far as the present case of $\sim 1.3 M_\odot$ star is concerned.

However, little can be said about higher mass stars based on our result alone. The apparent deficiency of O ($-0.5 \lesssim$ [O/Fe] $\lesssim 0$) reported by Takeda et al. (2008; cf. Fig. 12 therein), which appears to be enhanced with mass and correlated with a deficit in C ($-0.5 \lesssim$ [C/Fe] $\lesssim 0$) as well as an overabundance of Na ($0 \lesssim$ [C/Fe] $\lesssim +0.4$), was actually derived from red giants of low- through intermediate-mass ($1\ M_\odot \lesssim M \lesssim 5 M_\odot$). While Lagarde et al.'s (2012) calculations for solar-metallicity stars suggest a mass-dependent O-deficiency ([O/H] = $-0.004/-0.02$, $-0.03/-0.04$, $-0.04/-0.05$, $-0.07/-0.07$ corresponding to case 1/case 2 for 2, 3, 4, and 6 $M_\odot$, respectively), its extent is marginal and evidently insufficient to account for the trend suggested from Takeda et al.'s (2008) analysis based on the [O I] 5577 line. Whether or not the theoretical prediction reasonably explains the oxygen abundances also for red giants of higher-mass ($\sim$ 2–5 $M_\odot$) remains yet to be investigated.

6.5. Comparison with previous studies

Finally, we review the results of $\langle$[O/H]$\rangle$ (mean of M 67 stars) obtained in this study in comparison with those published by others, which are summarized in table 5. We can recognize from this table that both of our $\langle$[O/H]$\rangle$(giants) and $\langle$[O/H]$\rangle$(non-giants) are ~ 0.0 and thus consistent with the previous results based on high-quality data obtained by larger telescopes. Yet, we also note that the apparent star-to-star dispersion (standard deviation) of our O abundances is considerably large (0.19 dex for giants excepting S 1054 and 0.46 dex for non-giants) compared to literature values (mostly < 0.1 dex). This is apparently due to large errors involved in our abundance analysis where considerably low-quality data had to be invoked, which stems from the fact that our telescope and equipment were comparatively powerless from the viewpoint of the present-day standard.

As mentioned in section 1, it was our alternative aim to check how much information can be gained from our rather noisy spectra of medium resolution. We must admit here that the results we obtained are evidently insufficient for quantitatively discussing the detailed nature of abundances within the cluster (e.g., such as pursuing the degree of chemical homogeneity). We consider, however, that our study could serve as a useful pilot study to clarify the general qualitative tendency (e.g., consistency between the giant and non-giant groups at near-solar oxygen abundances) or to suggest an interesting candidate (S 1054) which may possibly have a peculiar oxygen composition. At any rate, we would stress the necessity of verifying what has been implied in this study, based on new observational data of much higher quality.

7. Conclusion

Despite the considerable progress in the study of abundance changes in the surface of red giants caused by evolution-induced dredge-up of nuclear-processed material, no consensus

has ever been accomplished yet about whether oxygen is significantly affected by such envelope mixing.

Give that the best approach to check if surface abundances suffer appreciable changes on the way to the red giant phase is to investigate cluster stars formed with the same composition, we carried out a spectroscopic study for selected 16 stars of M 67 in various evolutionary stages from the turn-off point through the red giant branch, along with Pollux, Procyon, and Sun (Ganymede) as reference stars.

The observations were done by using the 2-m NAYUTA telescope and the MALLS spectrograph at Nishi-Harima Astronomical Observatory, by which we could obtain moderate-dispersion ($R \sim 12000$) spectra (centered around $\sim$ 7700–7800 Å) for each star.

The atmospheric parameters were evaluated photometrically from colors ($T_{\rm eff}$), directly from mass and radius ($\log g$), and by using empirical formulas ($v_{\rm t}$).

We determined the oxygen abundances based on the synthetic spectrum-fitting in the 7770–7792 Å region comprising O I 7771–5, Fe I 7780, and Ni I 7788 lines. The non-LTE correction was further taken into account for deriving the final O-abundances.

In estimating abundance ambiguities involved in our analysis, errors due to noises as well as due to uncertainties in the adopted atmospheric parameters were taken into consideration. Regarding noise-related errors, we tried two independent determinations (application of a conventional formula to EW values and simulation by using many mock spectra with artificial noises) and compared with each other.

The abundances of Fe and Ni obtained as by-products were found to be roughly consistent with each other (though with a rather large dispersion) without any systematic trend.

It turned out that the mean oxygen abundances of M 67 stars are quite similar between the giant ($T_{\rm eff} < 5000$ K) and non-giant ($T_{\rm eff} > 5000$ K) groups at the near-solar composition (with only one exception of S 1054 which shows a marked O-deficiency by ~ 1 dex).

This result implies that oxygen content in the stellar envelope is almost unaffected by the mixing of H-burning products in the red-giant phase, as far as M 67 stars of low mass ($\sim 1.3 M_{\odot}$) are concerned, which is in agreement with the prediction from the conventional stellar evolution theory of first dredge-up.

S 1054 is a puzzling object. Although we can not completely exclude the possibility that its considerably low O-abundance is spurious (i.e., simply due to random fluctuation), a more detailed reanalysis based on high-quality data is needed.

The results we obtained based on rather noisy spectra of medium resolution (reflecting our use of smaller telescope) are not sufficient for quantitatively discussing the detailed nature of abundances within the cluster. Still, our study may be regarded as useful for a pilot study to clarify the general qualitative behavior of O abundances in M 67.

This research has made use of the SIMBAD database (operated at CDS, Strasbourg,

France) as well as the WEBDA database (operated at the Department of Theoretical Physics and Astrophysics of the Masaryk University).

References

Alonso, A., Arribas, S., & Martínez-Roger, C. 1995, A&A, 297, 197

Alonso, A., Arribas, S., & Martínez-Roger, C. 1996, A&A, 313, 873

Alonso, A., Arribas, S., & Martínez-Roger, C. 1999, A&AS, 140, 261 [Erratum: A&A, 376, 1039 (2001)]

Brown, J. A. 1985, ApJ, 297, 233

Cayrel, R. 1988, in The Impact of Very High S/N Spectroscopy on Stellar Physics, Proc. IAU Symp. 132, eds. G. Cayrel de Strobel & M. Spite (IAU), p. 345

Demarque, P., Woo, J.-H., Kim, Y.-C., & Sukyoung, K. 2004, ApJS, 155, 667

Eriksson, K., & Toft, S. C. 1979, A&A, 71, 178

Kurucz, R. L. 1993, Kurucz CD-ROM, No. 13 (Harvard-Smithsonian Center for Astrophysics)

Kurucz, R. L., & Bell, B. 1995, Kurucz CD-ROM, No. 23 (Harvard-Smithsonian Center for Astrophysics)

Kurucz, R. L., & Peytremann, E. 1975, Smithsonian Astrophys. Obs. Spec. Rept., No. 362

Lagarde, N., Decressin, T., Charbonnel, C., Eggenberger, P., Ekström, S., & Palacios, A. 2012, A&A, 543, A108

Mathieu, R. D., Latham, D. W., Griffin, R. F., & Gunn, J. E. 1986, AJ, 92, 1100

Mermilliod, J.-C. 1995, ASSL, Information & On-Line Data in Astronomy, 203, 127

Mishenina, T. V., Bienaymé, O., Gorbaneva, T. I., Charbonnel, C., Soubiran, C., Korotin, S. A., & Kovtyukh, V. V. 2006, A&A, 456, 1109

Ozaki, S., & Tokimasa, N. 2005, Annu. Rep. Nishi-Harima Astron. Obs., 15, 15 (in Japanese)

Pace, G., Pasquini, L., & François, P. 2008, A&A, 489, 403

Pancino, E., Carrera, R., Rosseti, E., & Gallart, C. 2010, A&A, 511, A56

Randich, S., Sestito, P., Primas, F., Pallavicini, R., & Pasquini, L. 2006, A&A, 450, 557

Sanders, W. L. 1977, A&AS, 27, 89

Sandquist, E. L. 2004, MNRAS, 347, 101

Shetrone, M. D., & Sandquist, E. L. 2000, AJ, 120, 1913

Takeda, Y. 1995, PASJ, 47, 287

Takeda, Y. 2003, A&A, 402, 343

Takeda, Y., Honda, S., Ohnishi, T., Ohkubo, M., Hirata, R., & Sadakane, K. 2013, PASJ, 65, 53

Takeda, Y., Kawanomoto, S., & Sadakane, K. 1998, PASJ, 50, 97

Takeda, Y., Ohkubo, M., Sato, B., Kambe, E., & Sadakane, K. 2005, PASJ, 57, 27 [Erratum: PASJ, 57, 415 (2005)]

Takeda, Y., & Sadakane, K. 1997, PASJ, 49, 367

Takeda, Y., Sato, B., & Murata, D. 2008, PASJ, 60, 781

Tautvaišienė, G., Edvardsson, B., Tuominen, I., & Ilyin, I. 2000, A&A, 360, 499

Tautvaišienė, G., Edvardsson, B., Puzeras, E., Barisevičius, G., & Ilyin, I. 2010, MNRAS, 409, 1213

Yong, D., Carney, B. W., & Teixera de Almeida, M. L. 2005, AJ, 130, 597

Table 1. Basic data of observed M67 stars.

Star	WEBDA	RA(2000)	DEC(2000)	V	$B-V$	$t_{\rm exp}$	S/N	Date	Remark
		(hour min sec)	(° ′ ″)	(mag)	(mag)	(sec)		(2014,UT)	
S 1279	164	08 51 28.991	+11 50 33.13	10.5379	1.1144	7200	130	Jan04	RGC
S 1010	141	08 51 22.804	+11 48 01.78	10.4675	1.0946	7200	70	Jan28	RGC
S 1074	84	08 51 12.697	+11 52 42.44	10.5221	1.0924	9600	120	Jan29+30	RGC
S 1084	151	08 51 26.181	+11 53 51.96	10.4929	1.0855	3600	75	Feb01	RGC
S 1054	104	08 51 17.028	+11 50 46.40	11.1393	1.0810	4800	95	Jan31	RGB binary?
S 1288	217	08 51 42.363	+11 51 23.09	11.2502	1.0714	9600	55	Feb02+03	RGB binary?
S 989	135	08 51 21.565	+11 46 06.20	11.4291	1.0702	8400	120	Feb22	Low GB
S 1277	218	08 51 42.314	+11 50 07.82	11.6221	1.0367	4800	25	Feb03	Low GB
S 1293	3035	08 51 39.386	+11 51 45.66	12.1223	0.9952	7200	65	Jan31	RGB binary?
S 1245	227	08 51 44.741	+11 46 46.03	12.9475	0.8925	6000	45	Jan31	SG
S 1056	96	08 51 15.639	+11 50 56.22	13.0015	0.8379	7200	20	Jan27	SG
S 489	7489	08 50 16.296	+11 53 48.00	12.7600	0.6800	13200	25	Jan28	TO gap
S 1034	115	08 51 18.541	+11 49 21.52	12.6530	0.6056	14400	25	Jan04	SG
S 1083	157	08 51 27.423	+11 53 26.56	12.7547	0.5678	6000	50	Jan27	TO
S 1270	241	08 51 49.143	+11 49 43.59	12.6843	0.5578	10800	40	Jan31	SG
S 1456	255	08 51 53.354	+11 48 20.89	12.7160	0.5181	10800	25	Jan28	TO

Note.

Most columns are self-explanatory. Each M 67 star, designated with the serial number assigned by Sanders (1977) and the reference number of WEBDA database (Mermilliod 1995; available at ⟨http://www.univie.ac.at/webda/⟩), is arranged as in table 2 (decreasing order in $B-V$, or increasing order in $T_{\rm eff}$). The positional data are taken from SIMBAD database, while the photometric data (V, $B-V$) are from Sandquist (2004). See section 2 for the derivation of S/N ratios presented in column 8. Given in column 10 is the evolutionary status classified by Sandquist (2004).

Table 2. Stellar parameters and the resulting abundances.

Star	$T_{\rm eff}$	$\log g$	[Fe/H]	$v_{\rm t}$	$A_{\rm O}^{\rm L}$	$\Delta_{\rm O}^{\rm N}$	$A_{\rm O}^{\rm N}$	$EW_{\rm O}$	$A_{\rm Fe}^{\rm L}$	$EW_{\rm Fe}$	$A_{\rm Ni}^{\rm L}$	$EW_{\rm Ni}$
Pollux	4904	2.84	+0.06	1.3	8.53	−0.10	8.43	25	7.47	135	6.56	133
S 1279	4668	2.45	+0.02	1.3	8.58	−0.09	8.49	20	7.45	140	5.94	109
S 1010	4705	2.44	+0.02	1.3	8.57	−0.09	8.48	21	6.90	108	5.64	91
S 1074	4709	2.47	+0.02	1.3	8.74	−0.10	8.64	25	7.11	119	6.08	116
S 1084	4722	2.46	+0.02	1.3	8.34	−0.08	8.26	16	7.78	162	6.95	172
S 1054	4731	2.73	+0.02	1.3	7.43	−0.06	7.37	3	7.78	162	6.77	154
S 1288	4749	2.78	+0.02	1.2	···	···	···	···	8.20	200	6.39	124
S 0989	4751	2.85	+0.02	1.2	8.53	−0.08	8.45	18	7.75	154	6.73	144
S 1277	4816	2.96	+0.02	1.2	8.97	−0.10	8.87	30	7.70	149	6.61	134
S 1293	4900	3.21	+0.02	1.0	8.74	−0.08	8.66	26	7.49	125	6.47	112
S 1245	5044	3.58	+0.02	0.9	8.64	−0.07	8.57	25	7.99	165	6.10	82
S 1056	5199	3.68	+0.02	1.0	···	···	···	···	···	···	7.22	147
S 0489	5703	3.79	+0.02	1.2	8.72	−0.15	8.57	57	···	···	5.93	54
S 1034	5975	3.84	+0.02	1.4	9.49	−0.35	9.14	128	7.07	80	6.80	90
S 1083	6123	3.93	+0.02	1.5	8.45	−0.16	8.29	63	6.89	67	5.80	28
S 1270	6163	3.92	+0.02	1.6	9.62	−0.44	9.18	155	7.96	130	6.96	94
S 1456	6329	3.98	+0.02	1.7	8.19	−0.16	8.03	56	8.13	137	6.29	45
Procyon	6612	4.00	−0.02	2.0	9.21	−0.37	8.84	148	7.38	87	6.53	47
Sun	5780	4.44	0.00	1.0	8.69	−0.09	8.60	48	7.74	124	6.61	81

Note.

In columns 1 through 5 are given the name (M 67 stars are indicated by Sanders numbers), effective temperature (in K), logarithmic surface gravity (in cm s^{-2}), metallicity (logarithmic Fe abundance relative to the Sun; in dex), and microturbulent velocity dispersion (in km s^{-1}) for each star. The LTE abundances ($A^{\rm L}$) resulting from our spectrum fitting analysis and the corresponding equivalent widths (EW; in mÅ) evaluated for O I 7774.17, Fe I 7780.55, and Ni I 7788.94 lines are presented in the remaining columns, where the non-LTE corrections ($\Delta_{\rm O}^{\rm N}$) and the non-LTE abundances ($A_{\rm O}^{\rm N}$) are also given regarding oxygen. All abundance results are expressed in the usual normalization of $A_{\rm H} = 12.00$.

Table 3. Comparison of the atmospheric parameters with the literature values.

Star	$T_{\rm eff}$ (K)	$\log g$ (cm s^{-1})	$v_{\rm t}$ (km s^{-1})	References
S 1279 (F164)	4700	2.50	1.8	Tautvaišienė et al. (2000)
	4668	2.45	1.3	This study
S 1010 (F141)	4730	2.40	1.8	Tautvaišienė et al. (2000)
	4700	2.30	1.34	Yong et al. (2005) (spectroscopic)
	4640	2.30		Yong et al. (2005) (photometric)
	4650	2.80	1.3	Pancino et al. (2010) (spectroscopic)
	4590	2.42	1.2/1.8	Pancino et al. (2010) (photometric)
	4705	2.44	1.3	This study
S 1074 (F84)	4750	2.40	1.8	Tautvaišienė et al. (2000)
	4709	2.47	1.3	This study
S 1084 (F151)	4760	2.40	1.7	Tautvaišienė et al. (2000)
	4722	2.46	1.3	This study
S 1034	6019	4.00	1.5	Randich et al. (2006)
	5975	3.84	1.4	This study

Table 4. Atomic data of the spectral lines used for abundance determinations.

Species	$\lambda_{\rm air}$ (Å)	$\chi_{\rm low}$ (eV)	$\log gf$ (dex)	Gammar (dex)	Gammas (dex)	Gammaw (dex)
O I	7771.944	9.146	+0.324	7.52	−5.55	(−7.65)
O I	7774.166	9.146	+0.174	7.52	−5.55	(−7.65)
O I	7775.388	9.146	−0.046	7.52	−5.55	(−7.65)
Fe I	7780.552	4.473	−0.066	7.88	−6.13	−7.80
Ni I	7788.936	1.951	−2.420	8.00	−6.31	−7.85

Note.

The first four columns are self-explanatory. Presented in columns 5–7 are the damping parameters: Gammar is the radiation damping width (s^{-1}) [$\log\gamma_{\rm rad}$], Gammas is the Stark damping width (s^{-1}) per electron density (cm^{-3}) at 10^4 K [$\log(\gamma_{\rm e}/N_{\rm e})$], and Gammaw is the van der Waals damping width (s^{-1}) per hydrogen density (cm^{-3}) at 10^4 K [$\log(\gamma_{\rm w}/N_{\rm H})$].

Most of these data were taken from the compilation of Kurucz and Bell (1995), though Kurucz and Peytremann's (1975) $\log gf$ value was adopted for Fe I 7780.552 as done in Takeda and Sadakane (1997) (cf. subsection 4.2). The parenthesized damping parameters are the default values computed by the WIDTH9 program, since the data are not available in Kurucz and Bell (1995).

Table 5. Mean oxygen abundances of M 67 stars derived by previous studies.

Ref.	Telescope	Type	N	Line	EW	S/N	R	$\langle$[O/H]$\rangle$ ($\pm\sigma$)	Remark
(1)	(2)	(3)	(4)	(5)	(6)	(7)	(8)	(9)	(10)
BRO85	2.7 m McDonald	RG	3	6300	26–39	70–100	25000	8.70* ($\pm$0.04)	Solar abundance unavailable
SHE00	2.7 m McDonald	BS	5	7773	84–296	44–75	30000	+0.11 ($\pm$0.31)	NLTE
SHE00	2.7 m McDonald	TO	4	7773	83–138	35–69	30000	+0.04 ($\pm$0.08)	NLTE
TAU00	2.6 m Nord. Opt. Tel.	RG	9	6300	3–6	$\gtrsim 100$	30000	$-$0.01 ($\pm$0.05)	$R \sim 60000$ data partly used
YON05	4.0 m KPNO/CTIO	RG	3	6300/6363	N/A	100–200	28000	+0.09 ($\pm$0.05)	
RAN06	8.2 m VLT	TO	10	6300	5–10	90–180	45000	+0.02 ($\pm$0.03)	
PAC08	8.2 m VLT	ST	5	6300	4–5	~ 80	100000	$-$0.04 ($\pm$0.08)	
PAN10	2.2 m Calar Alto	RG	3	6300	N/A	70–100	30000	+0.09 ($\pm$0.10)	Spectrum synthesis
TAKHON	2.0 m NAYUTA	RG	7	7773	16–30	25–130	12000	$-$0.05 ($\pm$0.19)	S 1054 excluded, NLTE
TAKHON	2.0 m NAYUTA	TO/SG	6	7773	25–155	25–50	12000	+0.03 ($\pm$0.46)	NLTE

Columns (1) through (10) gives the reference, used telescope, type of stars, number of stars, adopted line ("6300", "6363", "7773", means [O I] 6300, [O I] 6363, and O I 7771–5, respectively), equivalent-width range (in mÅ), S/N ratio range, resolving power, mean oxygen abundance relative to the reference solar abundance along with the standard deviation (in dex), and remarks (if any), respectively. Abbreviations used in columns (1) and (3) are denoted as follows:

(1): BRO85 ⋯ Brown (1985); SHE00 ⋯ Shetrone and Sandquist (2000); TAU00 ⋯ Tautvaišienė et al. (2000); YON05 ⋯ Yong et al. (2005); RAN06 ⋯ Randich et al. (2006); PAC08 ⋯ Pace et al. (2008); PAN10 ⋯ Pancino et al. (2010); TAKHON ⋯ this study.

(3): RG ⋯ red giants; BS ⋯ blue stragglers; TO ⋯ turn-off stars; ST ⋯ solar-type stars; SG ⋯ subgiants.

* $\langle A(\mathrm{O})\rangle$ (mean oxygen abundance) is presented here, since the reference solar abundance is unavailable.

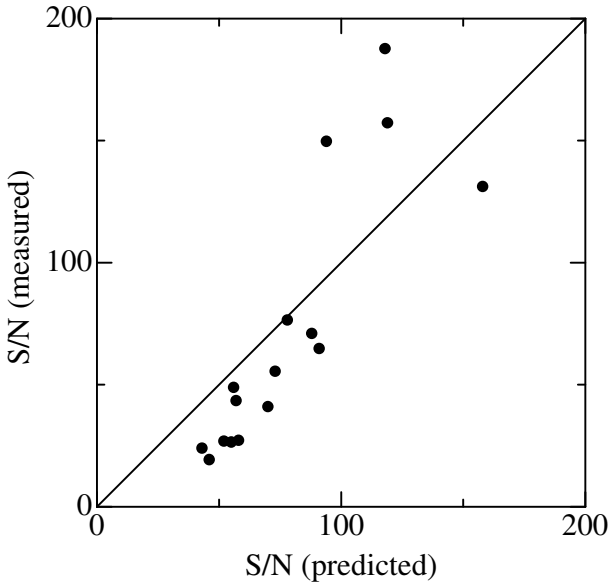

Fig. 1. Correlation between S/N(predicted) (evaluated from photon counts) and S/N (measured) (directly estimated from fluctuations at line-free windows) for 16 stars of M 67.

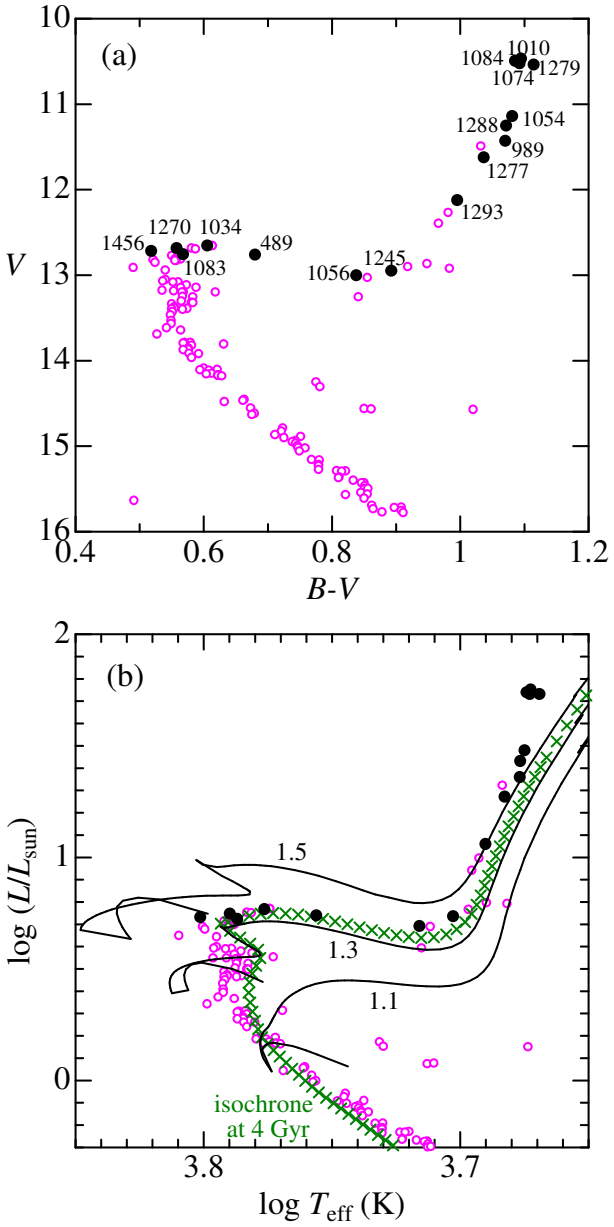

Fig. 2. (a) M 67 stars plotted on V vs. $B-V$ diagram, based on the photometric data taken from Sandquist (2004). Filled circles $\cdots$ our 16 targets (from the turn-off point through the red-giant branch). Open circles $\cdots$ other M 67 member stars which we did not observe. (b) M 67 stars plotted on the $\log L$ vs. $\log T_{\rm eff}$ diagram, with the same meanings of symbols as in panel (a). (See section 3 for the derivation of $T_{\rm eff}$ and L for each star.) The Yale–Yonsei theoretical solar-metallicity evolutionary tracks (corresponding to 1.1, 1.3, and 1.5 $M_{\odot}$) as well as the 4 Gyr isochrone (Demarque et al. 2004) are also depicted by solid lines and crosses, respectively.

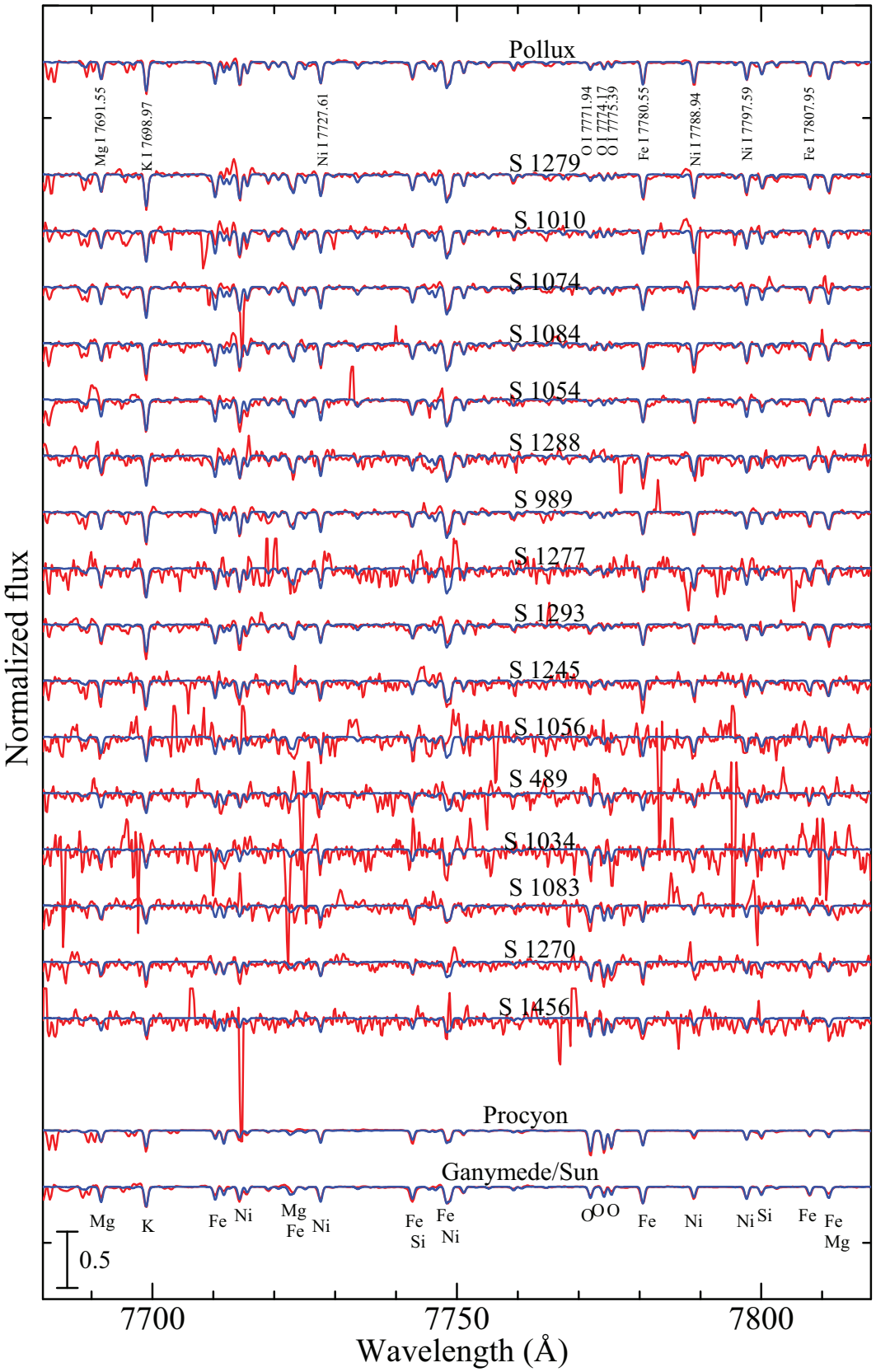

Fig. 3. Depicted in red lines are the observed spectra of 16 targets in M 67 (arranged in the order of increasing $T_{\rm eff}$ as in table 1), where theoretical spectra simulated with scaled solar abundances (see subsection 4.1) are overplotted in blue lines. The spectra of Pollux, Procyon, and Ganymede (substitute for the Sun) are also shown for comparison. The wavelength scale of each spectrum is adjusted to the laboratory system.

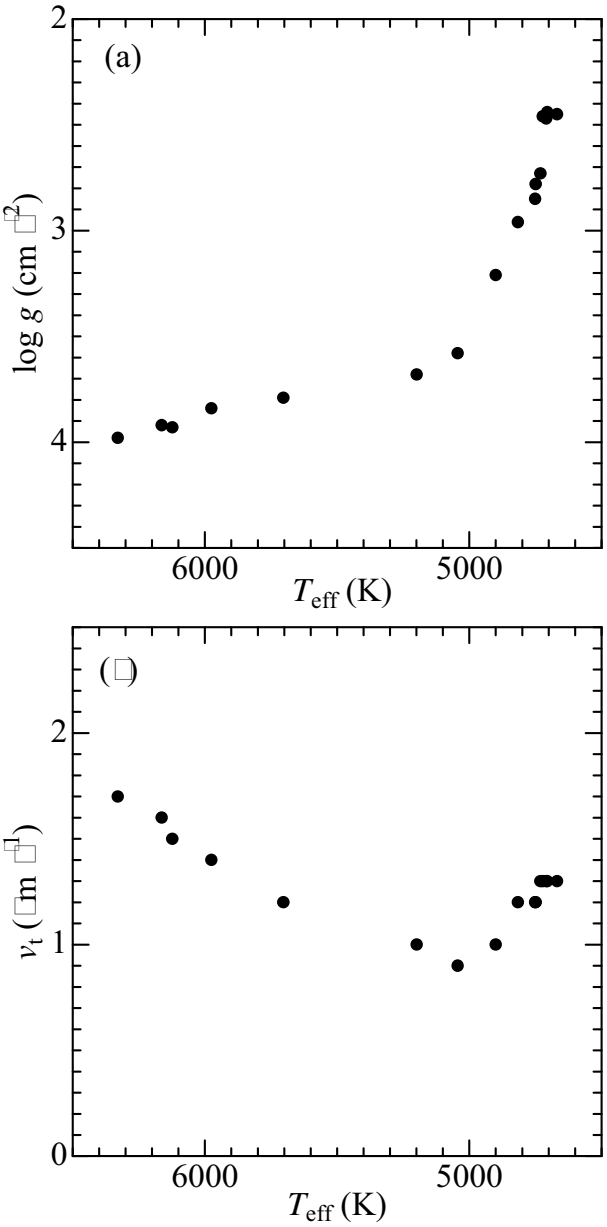

Fig. 4. $T_{\rm eff}$-dependence of (a) $\log g$ and (b) $v_{\rm t}$ for our 16 targets of M 67.

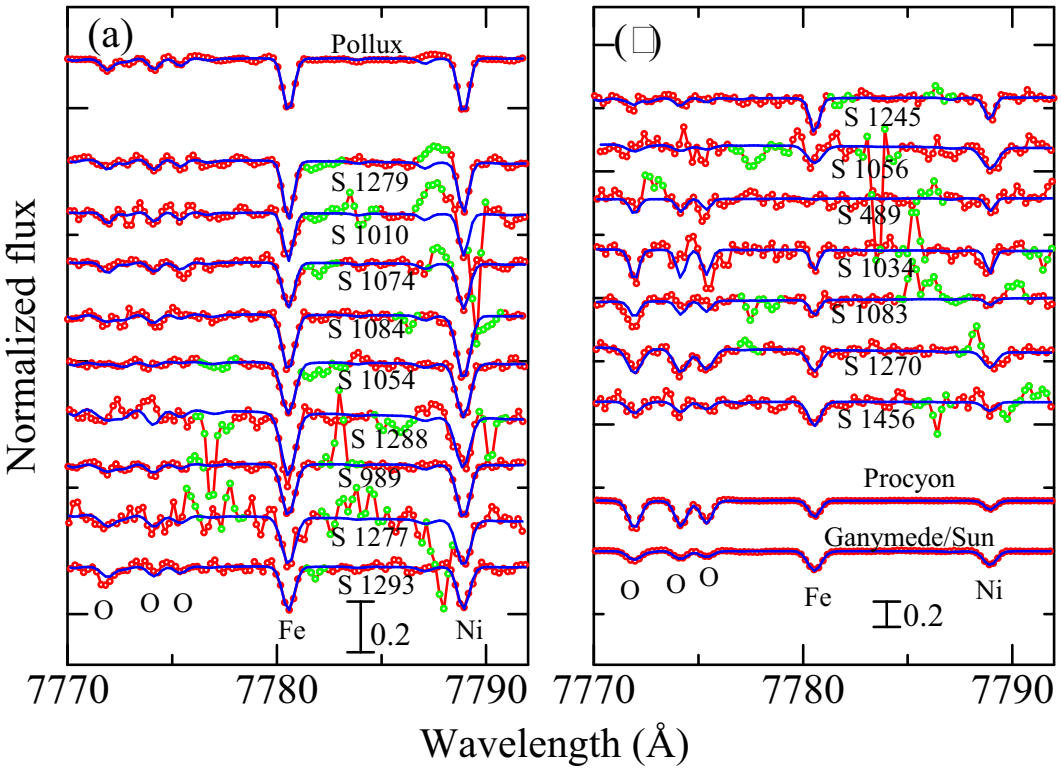

Fig. 5. Synthetic spectrum fitting in the 7770–7792 Å region comprising O I 7771.94, 7774.17, 7775.39, Fe I 7780.55, and Ni I 7788.94 lines. The best-fit theoretical spectra are shown by blue solid lines. The observed data are plotted by red symbols connected by lines, where those rejected in the fitting are highlighted in green. The spectra of M 67 stars are arranged (from top to bottom) in the order of increasing $T_{\rm eff}$, Note that the ordinate scale is twice as different in the left panel (giant stars) as in the right panel (non-giant stars). For the A(O)-indeterminable cases of S 1288 and S 1056, the theoretical spectra shown here were simulated with the fixed oxygen abundances at the metallicity-scaled solar composition.

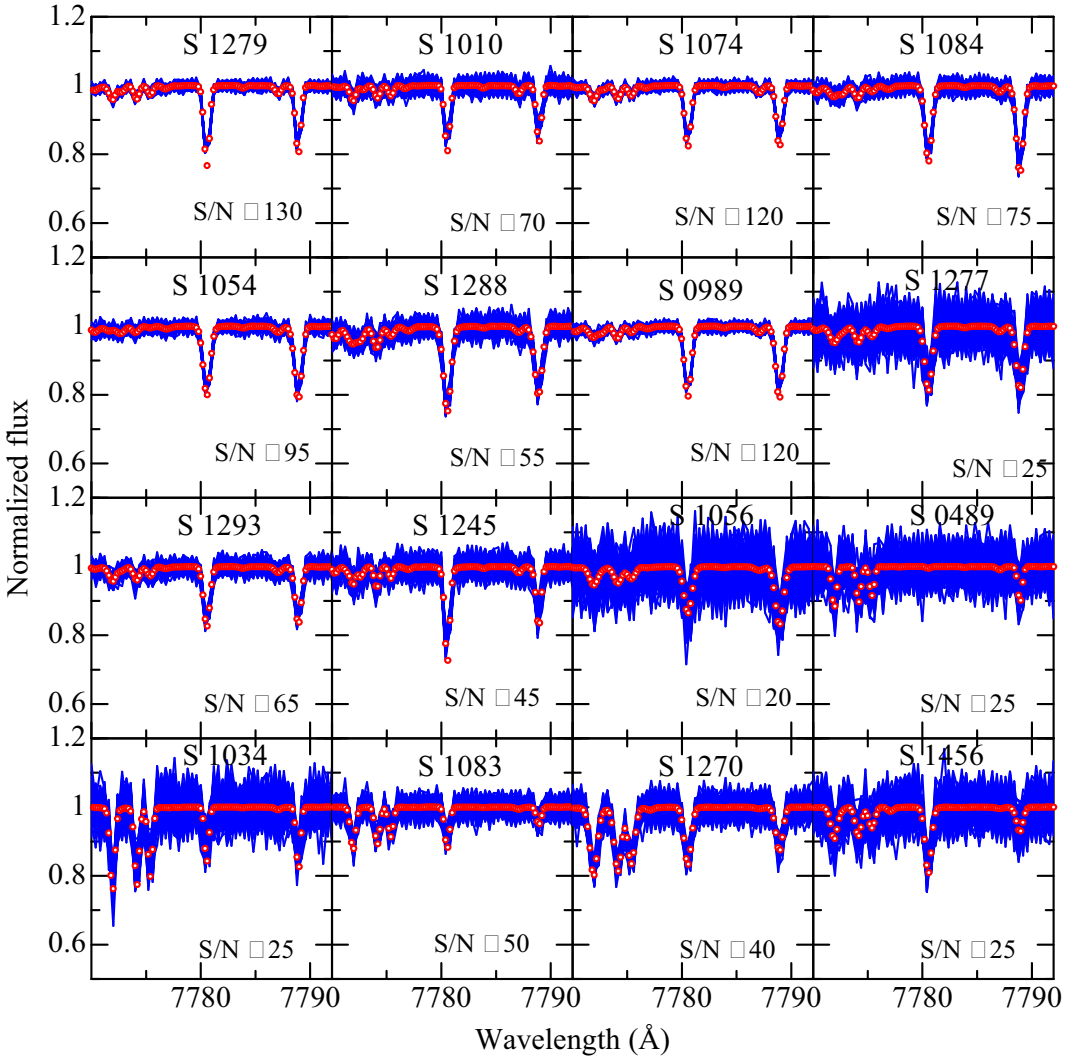

Fig. 6. Modeled spectra in the 7770–7792 Å region with artificial noises, for which spectrum-fitting analysis was formally performed to estimate abundance errors. Blue solid lines are overplotted mock spectra (100 for each star), generated by adding random noises (relevant for the S/N ratio) to the theoretical spectrum (red open circles) inversely computed based on the standard solutions of A(O), A(Fe), A(Ni), and $v_{\rm M}$.

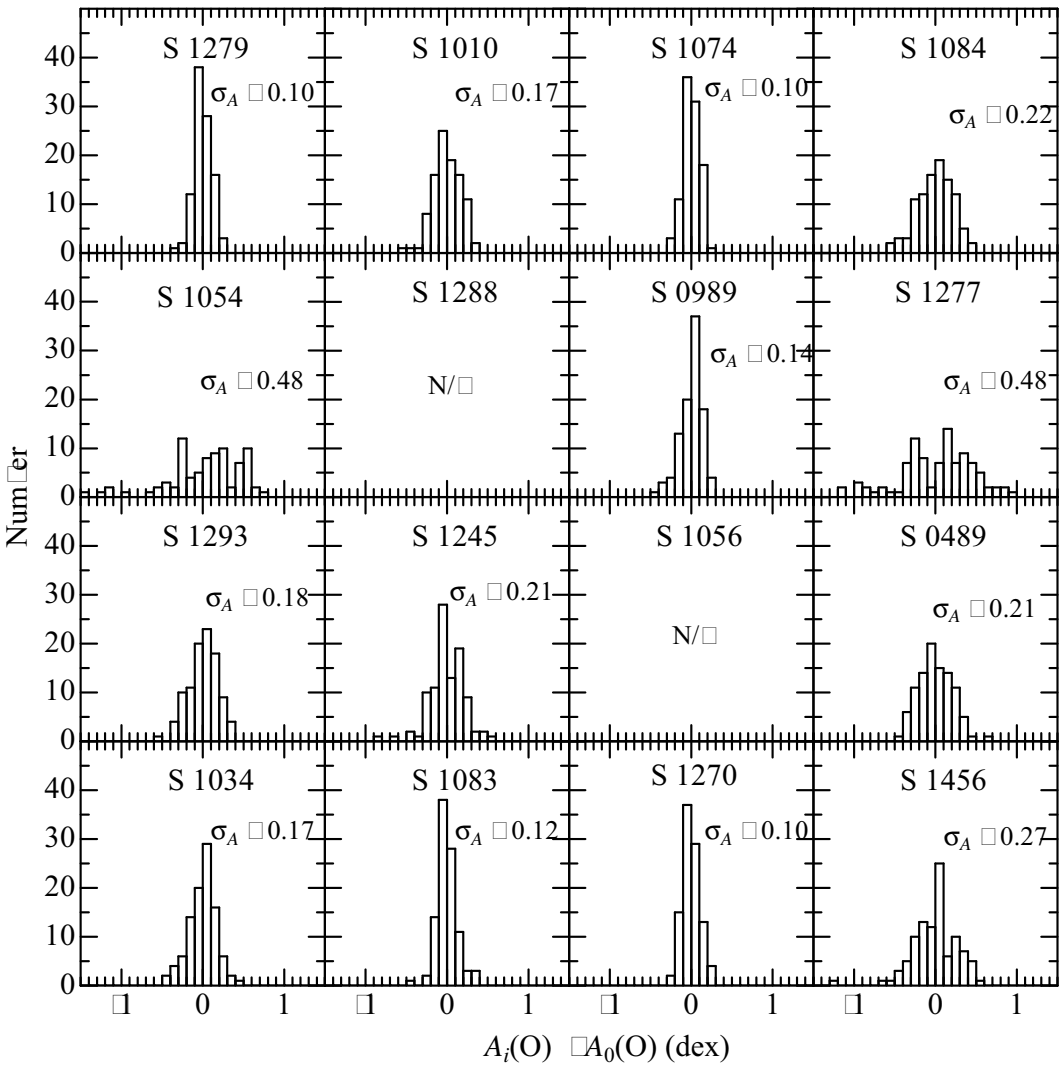

Fig. 7. Histogram of oxygen abundance deviations, which are defined as the differences between the apparent A_i(O) solutions (resulting from the fitting-analysis of 100 mock spectra with artificial noises; cf. figure 6) and the given A_0(O) used for modeling of the standard spectrum.

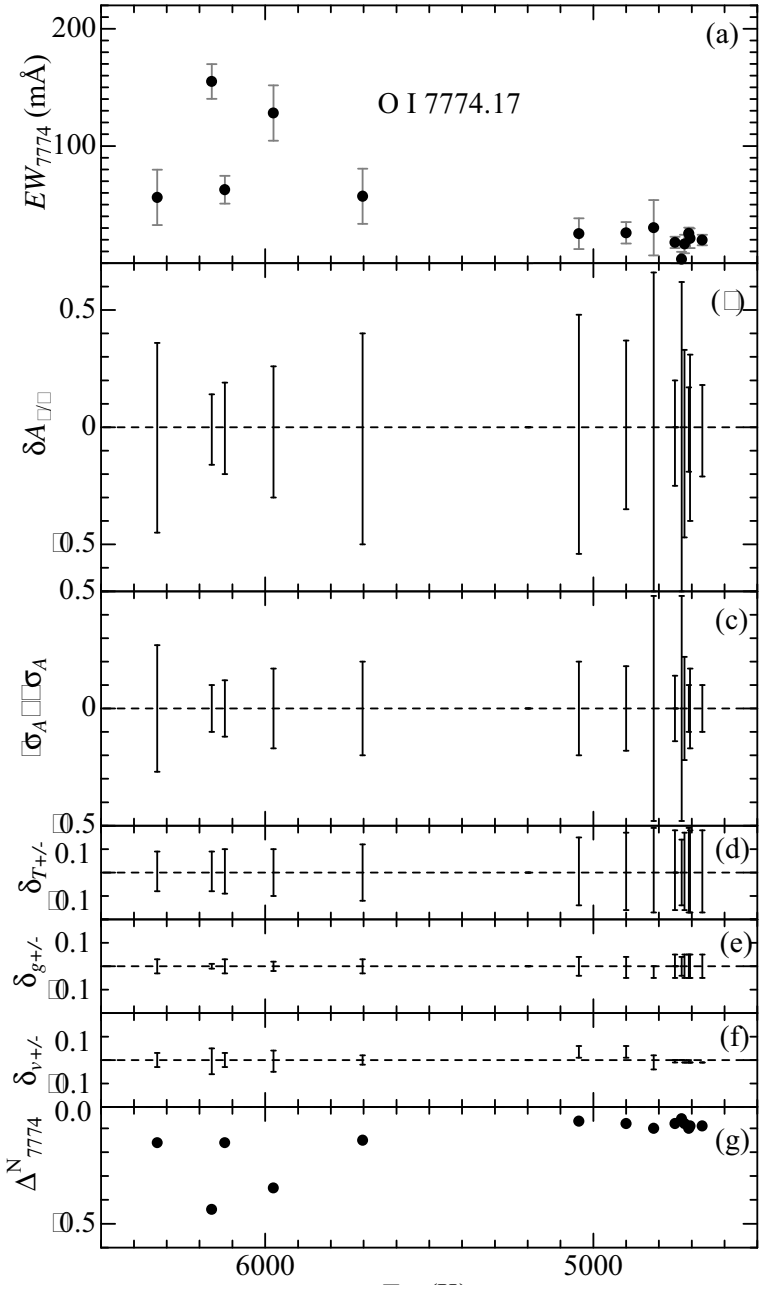

Fig. 8. Quantities related to O abundance errors plotted against $T_{\rm eff}$. (a) $EW^{\rm O}_{7774}$ (equivalent width of O I 7774.17) with EW ambiguity of $\pm\delta EW$ as error bars, (b) δA_+ and δA_- (abundance change corresponding to perturbation of $\pm\delta EW$), (c) standard deviation ($\pm\sigma$) of abundance differences resulting from the experiment based on 100 mock spectra with artificial noises, (d) δ_{T+} and δ_{T-} (abundance variations in response to $T_{\rm eff}$ changes of +2% and −2%), (e) δ_{g+} and δ_{g-} (abundance variations in response to $\log g$ changes of +0.1 dex and −0.1 dex), (f) δ_{v+} and δ_{v-} (abundance variations in response to perturbing $v_{\rm t}$ by +20% and −20%), and (g) $\Delta^{\rm O}_{7774}$ (non-LTE correction for O I 7774.17). Note that the same ordinate scales are adopted except for panel (a). The signs of δ's are $\delta_{T+}<0$, $\delta_{T-}>0$, $\delta_{g+}>0$, $\delta_{g-}<0$, $\delta_{v+}<0$, and $\delta_{v-}>0$.

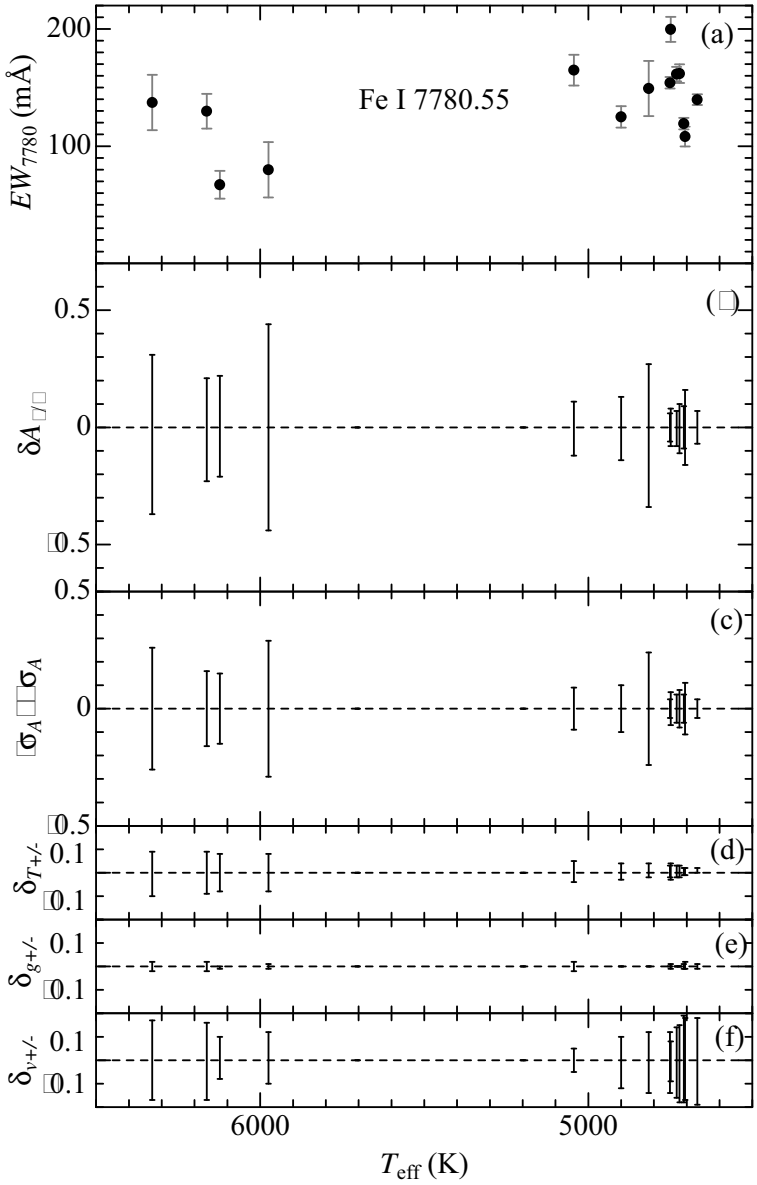

Fig. 9. Quantities related to Fe abundance errors plotted against $T_{\rm eff}$. While panel (a) shows $EW^{\rm Fe}_{7780}$ (equivalent width of Fe I 7780.55), the meanings of panels (b)–(f) are the same as in figure 8. The signs of δ's are $\delta_{T+} > 0$, $\delta_{T-} < 0$, $\delta_{g+} > 0$, $\delta_{g-} < 0$, $\delta_{v+} < 0$, and $\delta_{v-} > 0$.

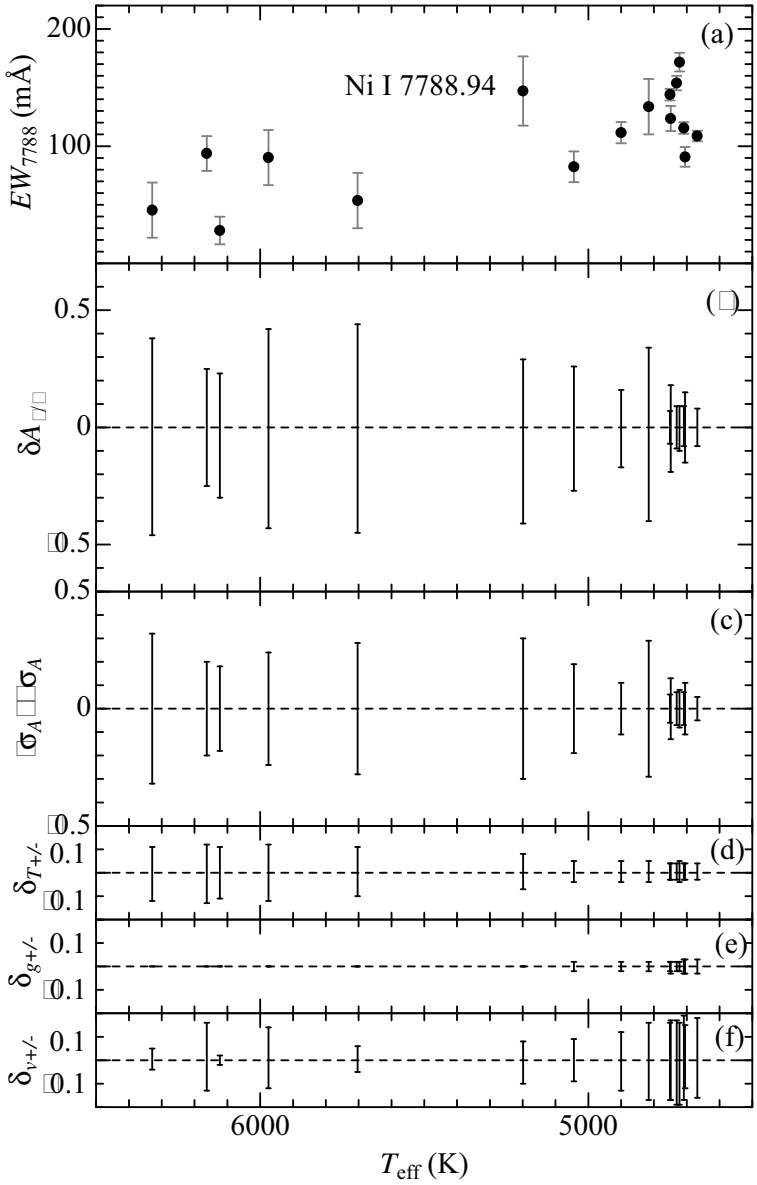

Fig. 10. Quantities related to Ni abundance errors plotted against $T_{\rm eff}$. While panel (a) shows $EW^{\rm Ni}_{7788}$ (equivalent width of Ni I 7788.94), the meanings of panels (b)–(f) are the same as in figure 8. The signs of δ's are $\delta_{T+} > 0$, $\delta_{T-} < 0$, $\delta_{g+} > 0$, $\delta_{g-} < 0$, $\delta_{v+} < 0$, and $\delta_{v-} > 0$.

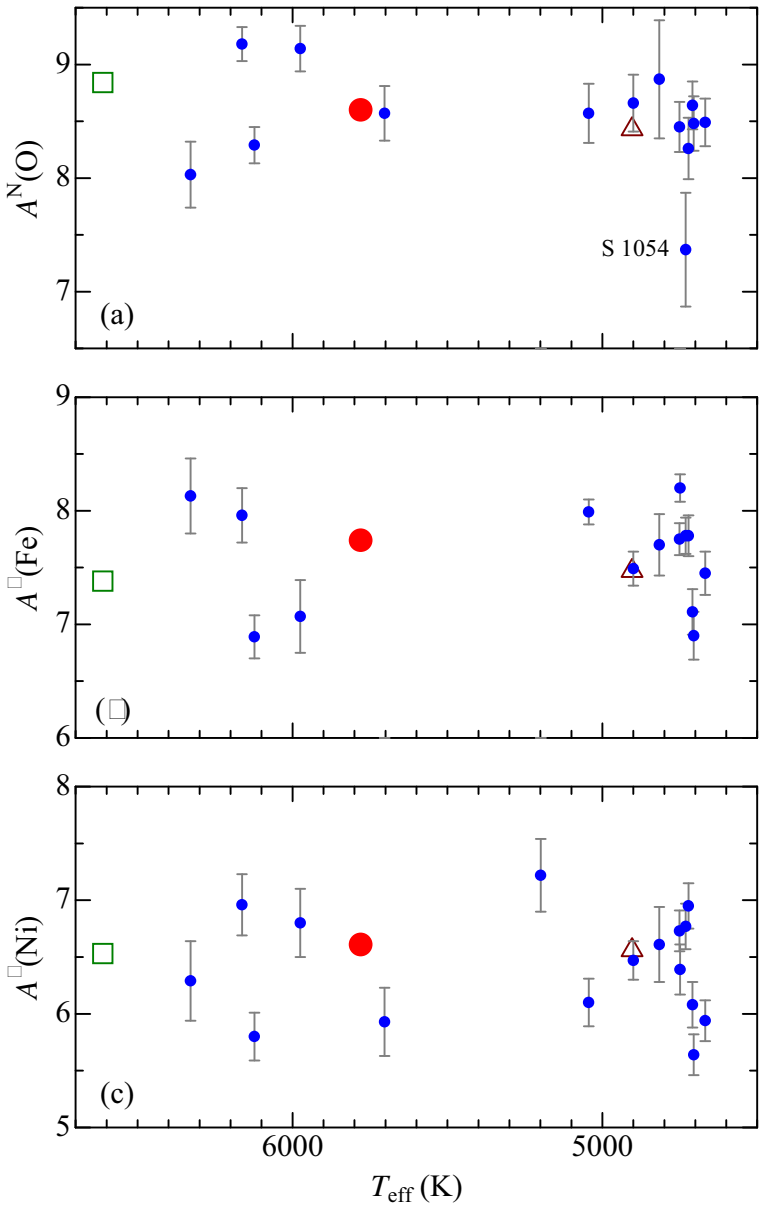

Fig. 11. Finally obtained abundances of (a) O, (b) Fe, and (c) Ni, plotted against $T_{\rm eff}$ The results for M 67 stars are shown in small symbols (blue filled circles), where the attached error bars are $\pm\sqrt{\sigma_A^2 + \delta_{Tgv}^2}$ (cf. subsection 5.4), while those for Pollux, Procyon, and the Sun are presented in large symbols (brown open triangle, green open square, and red filled circle, respectively).